Analysis of diabetes alteration of the mouse aorta from synchrotron micro-CT imaging

Xiaowen Liang, Aïcha Ben Zemzem, Sébastien Almagro, Timm Weitkamp, Laurent Debelle, Nicolas Passat

7th International Conference on Computational and Mathematical Biomedical Engineering - CMBE2021
27–29 June 2022, Italy
P. Nithiarasu and C. Vergara (Eds.)

ANALYSIS OF DIABETES ALTERATION OF THE MOUSE AORTA FROM SYNCHROTRON MICRO-CT IMAGING

Xiaowen Liang[1,2], Aicha Ben Zemzem[2], Sébastien Almagro[2], Timm Weitkamp[3], Laurent Debelle[2], and Nicolas Passat[1]

[1]Université de Reims Champagne Ardenne, CReSTIC EA 3804, 51100 Reims, France,
{xiaowen.liang,nicolas.passat}@univ-reims.fr
[2]Université de Reims Champagne Ardenne, CNRS, MEDyC UMR 7369, 51100 Reims, France,
{aicha.ben-zemzem,sebastien.almagro,laurent.debelle}@univ-reims.fr
[3]Synchrotron SOLEIL, 91192 Gif-sur-Yvette, France, weitkamp@synchrotron-soleil.fr

SUMMARY

Elastic lamellae are important extracellular matrix structures of the arterial wall. During aging and diabetes, they are strongly affected, losing their elasticity, resulting in increased arterial stiffness. Analyzing elastic lamellae geometry and organization is therefore of significance. We took high-resolution synchrotron X-ray microtomography images of mice aorta and segmented elastic lamellae fragments. We used those to measure and estimate the folding of these structures in healthy and diabetic mice. We discuss the choice of sampling parameters to better estimate the real length of elastic lamellae based on skeletonized images. We find that the measurements provide reliable evidence of elastic lamellae alterations due to diabetes.

Key words: *diabetes, mice aorta, elastic lamellae, microtomography, X-ray phase-contrast imaging, synchrotron, image segmentation, skeletonization, length estimation.*

1 INTRODUCTION

Diabetes is a chronic metabolic disease that consists of an increase in the concentration of glucose in the blood. Among other effects, this leads to the glycation of various molecules leading to the alteration of the stiffness of the artery by reducing the distensibility of the arterial wall [1]. The arteries of vertebrates are complex structures composed mainly of the lumen where the blood flows, surrounded by a wall made of a stack of elastic lamellae. In mice, the arterial wall consists of approximately five concentric elastic layers spaced by muscle cells. These elastic structures are mainly composed of elastin, a protein with a half-life of 70 years and whose re-synthesis is inefficient after adolescence. During diabetes, the addition of glucose to elastin alters elastic fibers and makes the artery more rigid. However, the exact impact of diabetes on elastic lamellae remains unclear, mostly because objective methods to address this point are unavailable. Aorta is a large elastic artery that is strongly affected by diabetes. The study of its fine structure requires a large field of observation, a high resolution and a 3D view to understand how the modifications occur on the whole volume. No conventional technique is able to combine these three characteristics. Two-photon and three-photon microscopy [2] are too limited in tissue thickness (0.5 and 1.3 mm depth, respectively), whereas the resolution of optical coherence tomography, echography and magnetic resonance imaging varies from tens of micrometers to millimeters. By contrast synchrotron X-ray microtomography (micro-CT) with in-line phase contrast, has been developed to visualize biological soft tissues with sub-micrometric resolution, several centimeters of tissue thickness and millimeter field of view. Recent works [3] exhibit these capabilities. Besides, some of the authors succeeded in discovering new arterial features inside the aortic wall [4]. The tomographic image data acquired on the ANATOMIX beamline of the SOLEIL synchrotron are 2048^3 voxel volumes, with a voxel size of 0.65 μm, leading to 32 GB per image. In these 3D grey-level images, it is possible to observe in the 2D slices the cross-section geometry of the elastic lamellae. Our purpose is to study the effect of the diabetes on the elastic lamellae of mouse aorta

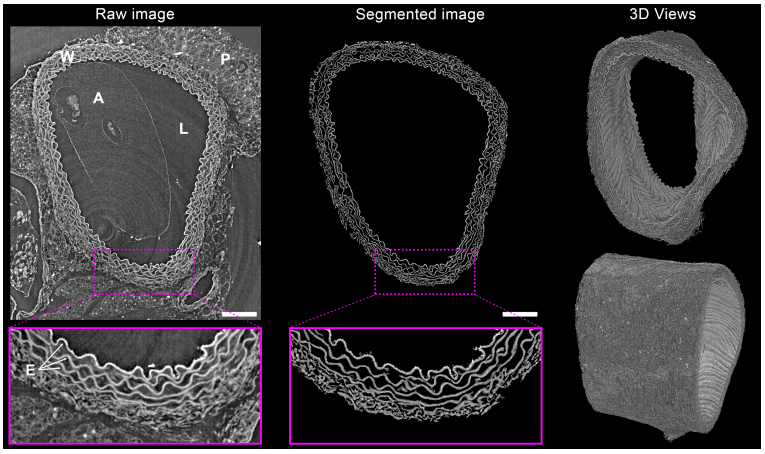

Figure 1: Synchrotron acquisition. Left – Raw image of C57Bl6J mouse (control). The artery wall (W) surrounds the lumen (L) of the aorta that contains agarose (A). Perivascular tissue (P) is linked to the external part of the arterial wall. Pink frame magnifies the wall where elastic lamellae (E) are stacked. Middle – The segmented image reveals elastic structures. Right – 3D views of reconstructed volume from 813 image slices (length : 528 μm, lumen diameter : 577 μm). Bars = 100 μm.

imaged from SOLEIL synchrotron. Elastic lamellae can be compared to a spring. Between two of its points, a spring has an "apparent" (Euclidean) length and a "curvilinear" (geodesic) length. The ratio between these two lengths expresses the ability of the spring to be stretched beyond its apparent length. In the remainder of this paper, we describe a morphometric study dedicated to quantify this length ratio and to assess the differences that occur between diabetic (*db/db* model) and control mice (C57Bl6J). These mice were all aged of 6 months (broadly similar to a 30 years human).

2 METHODOLOGY

2.1 Sample preparation

Aorta were collected after euthanasia, heart was injected by 2500 UI heparin. Heart and aorta were then washed with 10 mL PBS to remove residual blood. The aorta was then prefixed by injection of 5 mL of 4% formalin. 6 mL of 1% low melting agarose were injected to keep the aorta opened and to prevent collapse. Heart and aorta were both collected with surrounding tissues. Finally, the samples were fixed in 4% formalin for 24–48 hours, dehydrated and embedded in paraffin. The final samples were about 4-cm-long and 5-mm-wide paraffin rods containing the heart and aorta.

2.2 Imaging

Synchrotron X-ray microtomography was performed on the ANATOMIX beamline [5] at the SOLEIL synchrotron. Samples were imaged with a polychromatic ("white") X-ray beam obtained from an undulator X-ray source set to a gap of 8.5 mm; the beam was filtered by a 0.6-mm-thick diamond plate and a 10-μm-thick layer of gold. The detector was an indirect lens-coupled system with a 20-μm-thick lutetium aluminum garnet single-crystal scintillator coupled to a CMOS-based scientific-grade camera with 2048^2 pixels via microscope optics ($10\times$ objective), resulting in an effective pixel size of 0.65 μm on the sample level. The distance between sample and scintillator was 22 mm. The exposure time for the camera was set to 100 ms per projection image. 1500 projections were taken over an angular range of 180°. The samples were positioned vertically with the heart in the upper part. Immediately after the acquisition, the imaged volume was reconstructed and checked. Tomographic reconstruction was performed using the standard processing pipeline at the beamline, based on a Python script and subsequent reconstruction by the PyHST2 software [5]. The reconstructed volume stacks for each scan contained 2048^3 voxels of size $(0.65\ \mu\text{m})^3$, each represented by a 32-bit single-precision float value, i.e. a total of 32 GB per stack. After reconstruction, we manually controlled scans, and we eliminated invalid acquisitions due to sample preparation artifact (e.g. air bubbles). See Figure 1.

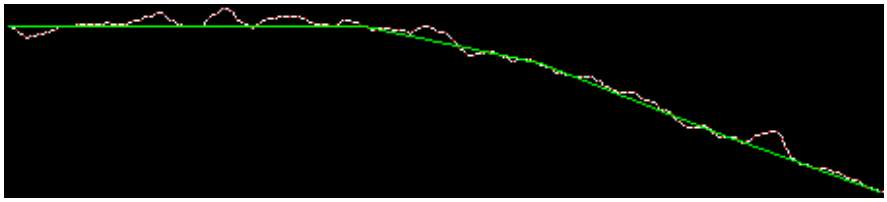

Figure 2: In white: a digital curve C obtained by the skeletonization of a segmented lamella in a 2D slice. In red: pixels sampled in C with a sampling parameter $s = 4$, inducing a polygon P (not depicted). In green: a "Euclidean-like" polygon that fits the curve by omitting the high frequency details, built from the vertices of P subsampled with a large sampling rate.

2.3 Image processing

In the 3D images, the elastic lamellae can be seen as surfacic objects globally oriented the same way as the wall of the artery (Figure 1, right). As a consequence, they appear as linear objects when observed in 2D slices of the images in the vessel cross-section plane (Figure 1, left). We study these linear objects from such 2D images. In this context, assessing the folding of 2D surfacic objects in 3D rewrites as assessing the tortuosity of the 1D linear objects in 2D. The lamellae are segmented from the 2D slices. Due to the good contrast of the images, the segmentation is carried out via the automatic Otsu method [6]. The binary result is skeletonized (and post-processed for pruning spurious branches of which the lengths are not longer than 10) in order to generate 1-pixel-width digital objects. These objects are split into curve segments that do not contain bifurcations, from which length estimators can then be relevantly computed.

2.4 Length analysis

In order to measure the tortuosity of a curve segment, two kinds of lengths are required: (1) a geodesic length $\mathcal{L}_{\text{geo}}$ that fits at best the trajectory of the curve, and (2) a Euclidean length $\mathcal{L}_{\text{Euc}}$ that only considers the global shape of the curve, i.e. that does not take into account its high frequency details. The tortuosity of a curve is then expressed as the ratio $\rho = \mathcal{L}_{\text{Euc}}/\mathcal{L}_{\text{geo}}$. In $\mathbb{R}^2$, we have $\rho \in (0, 1]$; the lower ρ, the more tortuous the curve. In a digital image, i.e. in $\mathbb{Z}^2$, the lengths $\mathcal{L}_{\text{geo}}$ and $\mathcal{L}_{\text{Euc}}$ can be estimated by considering a polygonal line P obtained by sampling the digital curve C. The computation of P from C depends on a sampling parameter $s \in \mathbb{N}^\star$. The vertices of P correspond to the points $\mathbb{Z}^2$, every s pixels in C. Each edge of P is then refined into s subsegments so that P finally contains a number of vertices equal to the number of pixels of C. See Figure 3. Let $\{V_i\}_{i=0}^{k}$ $(k > 0)$ be the vertices of P. The geodesic distance and the Euclidean distance are estimated as

$$\mathcal{L}_{\text{geo}} = \sum_{0 \leq i < k} \|V_{i+1} - V_i\|_2 \quad \text{and} \quad \mathcal{L}_{\text{Euc}} = \sum_{0 \leq j < \mathcal{L}_{\text{geo}}/\sigma,\ (j+1)\sigma \leq \mathcal{L}_{\text{geo}}} \|V_{(j+1)_\sigma} - V_{j_\sigma}\|_2 \qquad (1)$$

where V_{j_σ} is the nearest vertex to the point whose distance to the first vertex is $j.\sigma$ and $\sigma \gg 1$ is the sampling rate allowing to discard the high frequency details.

Parameters setting The length $\mathcal{L}_{\text{geo}}$ is computed from a digital curve that models an underlying real continuous curve. The difference between the true geodesic length of the real curve and the $\mathcal{L}_{\text{geo}}$ length of the digital one depends on two biases: the bias caused by the sampling (s) and the bias caused by the digitization ($\mathbb{R}^2$ to $\mathbb{Z}^2$). These two biases have antogonistic effects. In order to determine the sampling value s that is most likely to minimize the overall bias, we carried out experiments on synthetic digital curves of constant curvature $1/R$, i.e. circle segments of radius R of known length $R\theta$ where θ is the angular sector associated to the segment, with an algorithm previously used in radio astronomy [7]. We computed the mean ratio α between the digital geodesic length $\mathcal{L}_{\text{geo}}$ and the true length of the segments, for various radii $R \in [10, 30]$. The results are summarized in Table 1. We also investigated this ratio for straight line segments of size $S \in [20, 50]$ and we found that $|\alpha - 1| < 0.01$ when $s \geq 2$. These facts led us to choose $s = 4$ as sampling parameter. The sampling rate σ was empirically set to $\mathcal{L}_{\text{geo}}$ if $\mathcal{L}_{\text{geo}} \leq 100$; to $\mathcal{L}_{\text{geo}}/2$ if $100 < \mathcal{L}_{\text{geo}} \leq 300$; and to 100 if $300 < \mathcal{L}_{\text{geo}}$.

s	1	2	3	4	5	6	7	8	9
α	1.0551	1.0128	1.0046	0.9999	0.9955	0.9939	0.9907	0.9890	0.9842

Table 1: Mean value (α) of the ratios (computed for radii $R \in [10, 30]$) between the digital geodesic length $\mathcal{L}_{\text{geo}}$ and the true length of circular segments.

3 RESULTS AND PERSPECTIVES

We considered 21 3D images, partitioned in two groups: diabetic mice (11 images) and control mice (10 images). From each 3D image, we generated 2 000 to 3 000 curve segments. We computed the ratio ρ for these two groups. The results are depicted in Figure 3. For the chosen parameters (in particular, $s = 4$), the p-value of Mann-Whitney U test is $0.0035 < 0.05$. The difference between the mean values $\overline{\rho}_{\text{diabetes}} - \overline{\rho}_{\text{control}}$ is equal to 0.0662. In other words, the elastic lamellae in diabetic mice are globally flatter than those in control (i.e. healthy) mice. There is indeed a significant and quantifiable difference between the geometries of the elastic lamellae in diabetic and healhty mice. As a consequence the measure of elastic lamellae folding appears as a good indicator of the "actual" age of the artery, say the functional age of the arterial system rather than its chronological age.

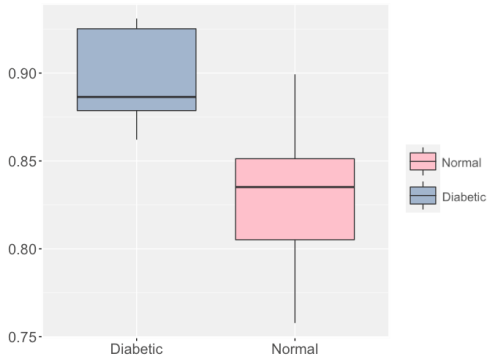

Figure 3: Box plot of ρ for the two groups (diabetic mice, in grey; control mice, in red) with $s = 4$.

ACKNLOWLEDGEMENTS

ANATOMIX is an Equipment of Excellence (EQUIPEX) funded by the Investments for the Future program of the National Research Agency, ANR, project NanoimagesX, grant ANR-11-EQPX-0031.

REFERENCES

[1] F. S. Vatner, J. Zhang, C. Vyzas et al. Vascular stiffness in aging and disease. *Frontiers in Physiology*, 12, 2021.

[2] X. Cheng, S. Sadegh, S. Zilpelwar et al. Comparing the fundamental imaging depth limit of two-photon, three-photon, and non-degenerate two-photon microscopy. *Optics Letters*, 45(10):2934–2937, 2020.

[3] J. López-Guimet, L. Peña-Pérez, R.S. Bradley et al. MicroCT imaging reveals differential 3D micro-scale remodelling of the murine aorta in ageing and Marfan syndrome. *Theranostics*, 8(21):6038–6052, 2018.

[4] A. Ben Zemzem, A. Genevaux, A. Wahart et al. X-ray microtomography reveals a lattice-like network within aortic elastic lamellae. *The FASEB Journal*, 35(10):e21844, 2021.

[5] T. Weitkamp, M. Scheel, J.L. Giorgetta et al. The tomography beamline ANATOMIX at Synchrotron SOLEIL. *Journal of Physics: Conference Series*, 849:012037, 2017.

[6] N. Otsu. A threshold selection method from gray-level histograms. *IEEE Transactions on Systems, Man, and Cybernetics*, 9:62–66, 1979.

[7] P. Zhang, P. Zucca, C. Wang et al. The frequency drift and fine structures of Solar S-bursts in the high frequency band of LOFAR. *The Astrophysical Journal*, 891: 89, 2020.